

The birth of the Milky Way: the in-situ halo and early thick disk as uncovered by accurate stellar ages with Gaia.

Carme Gallart^{1,2,*}, Edouard J. Bernard³, Chris B. Brook^{1,2}, Tomás Ruiz-Lara^{1,2}, Santi Cassisi^{4,5}, Vanessa Hill³, and Matteo Monelli^{1,2}

¹Instituto de Astrofísica de Canarias, E-38200 La Laguna, Tenerife, Spain

²Departamento de Astrofísica, Universidad de La Laguna, E-38205 La Laguna, Tenerife, Spain

³Université Côte d'Azur, Observatoire de la Côte d'Azur, CNRS, Laboratoire Lagrange, France

⁴INAF – Astronomical Observatory of Abruzzo, via M. Maggini, sn, 64100 Teramo, Italy

⁵INFN, Sezione di Pisa, Largo Pontecorvo 3, 56127 Pisa, Italy

⁶Laboratoire Lagrange, Université de Nice Sophia-Antipolis, Observatoire de la Côte d'Azur, CNRS, Bd de l'Observatoire, CS 34229, F-06304 Nice cedex 4, France

*carme@iac.es

As Milky Way-like galaxies form, smaller stellar systems accrete onto the main galactic progenitor, assembling a kinematically hot, spheroidal-like stellar halo surrounding the galactic disc^{1,2}. There is extensive observational evidence of this merging process both in the Milky Way and in external galaxies³⁻⁵. However, unambiguously identifying the oldest stellar population formed in the Milky Way main progenitor has remained elusive, as a good fraction of observed stars in our Galactic halo have characteristics pointing to an external origin⁶⁻⁸. In this paper, we unveil the old stellar population that can be associated with the first star formation events in the Milky Way. We identify this population with the red sequence of the enigmatic, double sequenced colour-magnitude diagram (CMD) of the kinematically hot, halo stars discovered in the second data release of the Gaia mission⁹. This discovery results from the novel, robust determination of stellar age distributions in the thick disc and halo Gaia CMDs, using the well established technique of CMD modelling^{10,11}, and the comparison with state-of-the-art cosmological simulations of galaxy formation¹². The age distributions unambiguously show that the stars in the blue and red sequences of the halo CMD are equally old, and older than the bulk of thick disc stars. This evidence allows us to identify the red sequence as the 'in-situ' halo stars, formed within the seed progenitor of our Milky Way. The in-situ halo is naturally more metal rich than the accreted halo population originating in the lower-mass galaxy Gaia-Enceladus whose stars form most of the blue sequence^{8,13}. These findings provide a crystal clear picture of the early sequence of events that gave rise to the complex Milky Way structure, and have far reaching implications for understanding the formation of disc galaxies in general.

Reliable ages for stars formed from the earliest star formation events to the present time are fundamental to understand the way that galaxies form and evolve. However, unlike velocities, apparent luminosities or colours, which can be directly measured from stellar spectra or images, obtaining stellar ages requires the comparison of observed properties with the predictions of stellar evolution models¹⁴. Obtaining unbiased age distributions for ensembles of stars is possible from the knowledge of their apparent luminosities and distances to convert these to absolute magnitudes, by applying the robust technique of colour-magnitude diagram (CMD) modelling. This technique has been used for over 20 years to determine detailed star formation histories for Local Group galaxies¹⁵⁻¹⁹. These galaxies are sufficiently close to observe

individual stars, yet far enough away that all their stars can be considered to be at the same distance, which can be obtained accurately using various well calibrated distance indicators^{20,21}.

However, applying this technique to populations of Milky Way stars had only been possible within an extremely small volume around the Sun^{22–25} owing to the difficulty of obtaining accurate distances for large stellar samples. This is one of the many aspects in which the Gaia mission is providing a breakthrough: in its second data release (DR2)²⁶, Gaia provided distances for 1.3 billion stars in the Milky Way. This distance information has allowed us, for the first time, to apply the CMD-fitting technique to the different morphological components of our own Galaxy and therefore to robustly derive their age distributions. This provides an unprecedented window to look at the early sequence of events that shaped the formation and structure of the Milky Way.

The top panels of Figure 1 show the CMD of two sub-populations of Milky Way stars taken from a parent population that lies within a sphere of 2 Kpc around the Sun, as observed by Gaia. The CMD in the top left panel contains about one hundred thousand stars from this spherical region with large tangential velocities relative to the Sun (greater than 200 km/s). These are the kinematically hot, halo stars. The CMD in the top right panel is of some one million stars from the same spherical region but selected to be at least 1.1 Kpc above and below the Galactic plane. At this distance from the plane, the majority of stars are expected to belong to the thick disc, rather than to the young thin disc component. We have excluded from this thick disc sample the stars with high velocity (greater than 200 km/s) that have been included in the halo CMD (see Methods for further information on the sample selection criteria). As is readily apparent, the CMD of the kinematically hot halo population contains two distinct sequences: a "blue" sequence on the left, and a "red" sequence on the right. This peculiar morphology indicates the presence of two distinct sub-populations within the halo. The blue sequence has been linked to a major accretion event, Gaia-Enceladus, which has been confirmed as the origin of an important fraction of stars in the inner Milky Way halo^{3,7,8,13}. However, the nature of the red sequence has been less clear. It has been associated with the Milky Way thick disc¹³, with support for this association coming from the characteristics of its chemical composition⁷. However, this interpretation does not explain the hot kinematic properties of this stellar population.

We have compared the distribution of stars in these observed CMDs with that in CMDs computed with state-of-the-art stellar evolution models²⁷ and found the combination of ages and chemical composition (metallicities) of the stars that best reproduce the observed CMDs (see Methods). These best-fit CMDs are displayed in the bottom two panels of Figure 1. The model CMDs clearly succeed at reproducing the various features observed in the empirical CMDs.

Figure 2 displays the distribution of ages and metallicities of these best-fit model CMDs, divided in the blue and red sequences in the case of the halo CMD. The age distributions clearly demonstrate that the two sequences in the halo CMD are composed by stars that are coeval and formed at the earliest possible times in the life of the Universe (peak age 13.4 Gyr, 50% of stars formed by 12.3 Gyr ago). The difference in colour is a result of the red and blue sequence stars having different metallicities. The models also clearly show that the thick disc population is younger than the two halo populations (peak age 8.7 Gyr, 50% of stars formed by 9.3 Gyr ago).

These age results contrast with previous ages assigned to stars associated with these components^{7,28} on which previous conclusions on their nature relied⁸. However, these earlier age determinations were based either on i) a relatively small number of stars, and used spectroscopically determined stellar parameters which allow less robust age estimates than absolute luminosities and colours⁷ or ii) indirect age estimates based on low resolution spectroscopy²⁸.

Our age determinations provide crucial insight into the formation of the Milky Way. Firstly, the well established relation²⁹ between a galaxy's mass and the amount of metals (defined as chemical elements

other than Hydrogen and Helium) contained in its stars means that the stars in the red sequence of the halo, being more metal rich, must have formed in a galaxy that was more massive than the one where the stars in the blue sequence were formed. Secondly, the fact that the two halo populations are coeval means not only that the red and blue populations formed stars at similar times, but that they also stopped forming at similar times. Both these findings are precisely what is expected if these two populations were involved in a merger event, with the red sequence stars belonging to the main progenitor of the Milky Way, and the blue sequence belonging to a smaller accreted galaxy, the one dubbed Gaia-Enceladus. This is shown in Figure 3. The left panel shows the age-metallicity distribution derived from the observed CMDs, with the red and blue sequence halo stars indicated as red and blue contours. The right panel shows the signature in the age-metallicity plane left by a merger event in a simulated Milky-Way analogue galaxy (see Methods), where the main progenitor stars are shown as red contours and the accreted galaxy as blue contours. The merger can be identified as two tracks in this plot, with the higher metallicity stars belonging to the main progenitor and the lower metallicity stars coming from the less massive merged galaxy.

The difference in the amount of metals in the red and blue sequences indicates that the accreted Gaia-Enceladus had about 30%³⁰ of the mass of stars in the main progenitor, although we stress that this ratio remains quite uncertain. This would indicate a total mass ratio of around 4:1 between the two galaxies, given the relation between stellar mass and total mass³¹. This estimated mass ratio is similar to that derived in previous works⁸ using different arguments. Regardless of the exact mass ratio, this encounter heated some of the main progenitor stars that had been forming in a disc-like structure, to the extreme kinematics that lead them to be classified as halo stars. The existence of such halo stars that were born 'in-situ' in the main progenitor, and then heated by accretion events, has been predicted by cosmological simulations of Milky Way-type galaxies^{32,33}, but such stars have not previously been identified.

The similar star formation timescales for the two halo sequences also has important implications for the origin of their detailed chemical enrichment. It is known^{7-9,13} that for stars with similar amounts of Fe, the blue sequence stars (Gaia-Enceladus) have significantly less α -elements than the red sequence stars (formed in the main progenitor). The run of $[\alpha/\text{Fe}]$ vs. $[\text{Fe}]$ in different stellar systems is commonly used to trace the star formation timescale of a galaxy, since α elements are produced in Supernova Type II on shorter timescales than iron, which is mostly produced on a longer timescale by Supernovae Type Ia. Our results indicate that other mechanisms should be at play, such as different star formation rate³⁴ or/and preferential outflows of metal enriched gas in the lower mass accreted galaxy. Indeed, the latter mechanism is occurring in the simulated Milky Way analogue galaxy, and is the origin of the differences in α abundances between the main progenitor and accreted system.

A further interesting result is the relation between the red sequence, or 'in-situ' halo, and the thick disc. The CMDs of these two components overlap, as seen in Figure 1, as do their ages, chemical abundances and kinematics as seen in Figures 2 and 4 as well as in previous studies^{9,13,35,36}. The implication is that the in-situ halo and thick disc have the same origin, linked to the main progenitor of the present day Milky Way: in this self consistent scenario, the old age tail of the thick disc population shown in Figure 2 is populated by stars formed in the main progenitor, which were not heated to halo-like velocities. Therefore, stars that would be currently associated to the thick disc were forming in the main progenitor before, during and after the merger with Gaia-Enceladus, whilst a fraction of main progenitor stars formed very early, were heated to halo kinematics by the accretion event. Such a formation scenario of the thick disc has been foreshadowed by cosmological galaxy formation simulations³⁷: the thick disc forms at high redshift during a period characterised by gas rich mergers.

A final implication of our findings regards the transition^{38,39} between thick and thin disc formation. The derived ages for thick disc stars indicate that this transition occurred around 8 Gyr ago, in agreement

with previous studies⁴⁰ and that this transition was not associated with the earlier Gaia-Enceladus merger.

In conclusion, the reported new observational results, aided by state-of-the-art cosmological simulations of disc galaxy formation, delineate a clear picture of the formation of our Galaxy. In this picture, a primitive Milky Way had been forming stars during some 2.5 Gyr when a smaller galaxy, which had been forming stars on a similar timescale but was less chemically enriched owing to its lower mass, was accreted to it. This merger heated part of the existing stars in the main progenitor to a stellar halo-like configuration. A ready supply of infalling gas during the merger ensures the maintenance of a disc-like configuration, with the thick disc continuing to form stars. Our measured age distributions indicate that the thick disc reached its peak star formation rate around 9 Gyr ago, that is 4.5 Gyr after the first stars formed in the Milky Way. Subsequently, around two Gyr later, the gas settled into a thin disc that has continued to form stars until the present day.

Acknowledgements CG, TRL and MM acknowledge support by the Spanish Ministry of Economy and Competitiveness (MINECO) under the grants AYA2014-56795-P and AYA2017-89076-P as well as AYA2016-77237-C3-1-P (TRL). SC acknowledges support from Premiale INAF "MITIC" and has been supported by INFN (Iniziativa specifica TAsP). We used data from the European Space Agency mission Gaia (<http://www.cosmos.esa.int/gaia>), processed by the Gaia Data Processing and Analysis Consortium (DPAC; see <http://www.cosmos.esa.int/web/gaia/dpac/consortium>). Funding for DPAC has been provided by national institutions, in particular the institutions participating in the Gaia Multilateral Agreement. We also used data from the LAMOST and GALAH surveys. Guoshoujing Telescope (the Large Sky Area Multi-Object Fiber Spectroscopic Telescope LAMOST) is a National Major Scientific Project built by the Chinese Academy of Sciences. Funding for the project has been provided by the National Development and Reform Commission. LAMOST is operated and managed by the National Astronomical Observatories, Chinese Academy of Sciences. The GALAH survey is based on observations made at the Australian Astronomical Observatory, under programmes A/2013B/13, A/2014A/25, A/2015A/19, A/2017A/18. We acknowledge the traditional owners of the land on which the AAT stands, the Gamilaraay people, and pay our respects to elders past and present.

Correspondence and requests for materials should be addressed to CG (carme@iac.es).

Methods

1 Data selection

A detailed and reliable determination of the age and metallicity distributions of a stellar system can be obtained from a CMD that is essentially complete down to the oldest main sequence turn-offs¹⁰. For a relatively metal-rich stellar population such as that of the Milky Way, the old turnoff occurs at an absolute magnitude $M_G=4$ in the Gaia G band, but it is necessary to reach about one magnitude deeper to accurately sample this critical point in the CMD. At a distance of 2 Kpc from the Sun, $M_G=5$ corresponds to an apparent magnitude $G=16.5$, down to which Gaia DR2 is essentially complete.

From Gaia DR2²⁶ we selected all the stars inside a sphere of radius 2 Kpc centered in the Sun down to $M_{G,R}=7$ (where $M_{G,R}$ stands for M_G before applying any correction for interstellar extinction; stars with two magnitudes in excess of the required $M_G=5$ were initially selected in order to retain highly reddened stars). $M_{G,R}$ was calculated directly from the apparent magnitude using the Gaia parallaxes, as $M_G=G+5+5\times\log_{10}(\omega/1000.0)$, with ω being the parallax in milliarcseconds. This transformation is valid because the great majority (over 80%) of these selected stars within the 2 Kpc sphere have small relative parallax error ($\text{parallax_over_error} > 5$ ⁴⁴). Following⁹, it was also required that $\text{astrometric_chi2_al}/(\text{astrometric_n_good_obs_al} - 5) < 1.44\times\max(1, \exp(-0.4\times(\text{phot_g_mean_mag}-19.5)))$ (only 2% of stars were removed by this cut) and that the stars had $(G_{BP}-G_{RP})$ measured colour. Corrections for interstellar extinction were calculated on a star by star basis by interpolating the colour excess from a 3-D map⁴⁵. We used published extinction coefficients⁴⁶, together with the effective temperature of each star. The latter was estimated using the correlation between $G_{BP}-G_{RP}$ colour and temperature T_{eff} determined from a large sample of Gaia DR2 stars with measured T_{eff} .

From this parent population, we selected as thick disc sample all the stars in the North and South caps of the sphere, with distances from the Galactic plane, $|Z| > 1.1$ Kpc, and tangential velocities, calculated as $V_T=(4.74/\omega)\times\sqrt{\text{pmra}^2 + \text{pmdec}^2}$, lower than 200 km/s. For the halo sample, we selected all the relatively high Galactic latitude stars ($b>30$) with $V_T > 200$ km/s. The latitude cut was performed to avoid substantial contamination from the thin disc at low galactic latitude. After keeping only stars brighter than $M_G=5$, the thick disc sample contains 836,937 stars and the halo sample contains 86,008 stars. The CMD of these stellar samples are displayed in the top panels of Figure 1.

2 Modelling of the CMD

In order to derive age and metallicity distributions of each population, the observed CMDs have been modelled through the comparison with synthetic CMDs following a state-of-the-art theoretical framework^{18,27,47}. In this process, the combination of simple stellar populations (that is, synthetic populations with small ranges of ages, $\Delta T \leq 1$ Gyr, and metallicities, $\Delta [\text{Fe}/\text{H}] \sim 0.1$ dex) which provide the best fit is obtained. The minimization has been performed with the code *TheStorm*^{11,48}. This code uses a *mother* synthetic CMD from which the simple stellar populations are extracted. These synthetic CMDs have been calculated using the BaSTI stellar evolution library in its solar-scaled⁴⁹¹ and α -enhanced heavy element distribution versions²⁷. For the comparison itself, we make use of most of the area within the CMD populated by stars, excluding the Horizontal Branch (HB) which is still difficult to reproduce quantitatively in stellar evolution models. Although this portion of the CMD is not included in the CMD fit, we tried to obtain a fine match of this evolutionary stage in the observed CMDs of both the halo -where it is quite

¹The whole set of stellar models used for present work are available at the following URL: <http://basti.oa-abruzzo.inaf.it>

prominent- and the thick disc -where the blue extension of the HB is basically missing. Since, for any given metallicity, the HB morphology is mainly driven by the mass loss efficiency during the red-giant branch stage, we used stellar model sets accounting for different efficiency of this process appropriate for each component: we used $\eta=0.2$ for simulating the thick disc CMD and $\eta=0.4$ for the halo CMD, where η is the free parameter used in combination with the Reimers' mass loss law in stellar modelling²⁷. Although different η values have been chosen for the different components under analysis, we should state that the results presented in this paper are not contingent upon this particular choice. Common to all *mother* synthetic CMDs (with 10^8 stars) are a constant star formation rate with flat age and metallicity distributions (14 Gyr to 30 Myr, and $-2.6 < [\text{Fe}/\text{H}] < 0.1$) and the Kroupa initial mass function⁵⁰. A binary fraction of 0.7 with mass ratio q uniformly distributed between 0.1 and 1 has been adopted. The results displayed in Figures 1, 2, and 3 are obtained with the α -enhanced models, which are the most adequate for thick disc and halo stellar populations. However, we note that our conclusions are not affected by the choice of a scaled-solar heavy element distribution. Finally, stellar evolutionary model predictions have been transferred to the Gaia photometric system by using appropriate bolometric correction tables using the prescriptions for the DR2 catalogue⁵¹.

Prior to the comparison between the observed Gaia CMDs and the *mother* synthetic CMDs, it is necessary to perform a simulation of the observational errors in the synthetic CMD, in such a way that it can be consistently compared with the observations. We have considered two error sources, namely: the error in the absolute magnitudes introduced by the error in the parallax, and the error in the Gaia photometry. To model the first error source, which dominates the error in M_G , we have statistically reproduced the distributions of `parallax` and `parallax_over_error` of the observed sample in the synthetic CMD. Then, the theoretical M_G values are transformed to account for observational errors by adding a correction given by a Gaussian distribution centred at 0 and with a standard deviation given by $\Delta M_G = 2.17 / \text{parallax_over_error}$. Similarly, the errors in the Gaia photometry have been implemented by adding a dispersion of 0.004 magnitudes to the $(G_{BP} - G_{RP})$ colour of all synthetic stars at all magnitudes⁵¹.

The comparison between the observed and synthetic CMDs is performed using the number of stars in small colour-magnitude boxes. No a-priori constraint on the age-metallicity relation is adopted: *TheStorm* code solves simultaneously for age and metallicity within the range covered by the simple stellar populations. For more details on the fitting procedure and error calculation, the reader is referred to published references^{11,18,52}.

The results of this CMD fitting process are the star formation rate as a function of time and the age-metallicity distribution. From these, it is possible to compute a best-fit CMD (displayed in the lower panels of Figure 1) which is then used to derive the age and metallicity distributions displayed in Figures 2 and 3 (panel a). In the case of the halo CMD, the fitting process has been performed in the CMD including both the blue and the red sequences. The age and metallicity distributions presented in Figure 2 separately for each sequence have been derived by drawing a polygon enclosing each sequence in the observed CMD (avoiding the red clump where both sequences naturally overlap) and using this polygon to assign synthetic stars in the best fit CMD to either the blue or the red sequence. The boundary between the blue and red sequences corresponds to the fiducial line shown in Figure 1. We have tested that this particular delimitation has a negligible impact on the results presented here.

3 Cross-match with spectroscopic surveys

We used a homogeneous catalogue⁴³ of distances, 3-D velocities, and ages for the cross-match between major Milky-Way spectroscopic surveys and Gaia DR2. We have used this catalogue, together with the

original Gaia DR2 information and the original [Fe/H] information from LAMOST third data release A, F, G, K catalogue <http://dr3.lamost.org/> (`feb` value)⁴¹ and GALAH first data release (`fe_h` value)⁴², to select stars matching exactly the same spatial and kinematical selection as our CMDs. The cross-identifications were performed requiring exact match of the corresponding identification numbers in the different catalogues (Gaia `source_id`, LAMOST `obsid` and GALAH `gaia_dr2_id`). We selected these two surveys because i) LAMOST includes a significant number of stars on the main-sequence turnoff region of the CMD overlapping with our halo sample (2,588 stars after quality cuts, see below), and with our thick disk sample (31,810 stars). SEGUE also has a significant overlap in the main sequence region, but the survey target selection function somehow selected mostly stars on the blue main sequence. The other two high resolution surveys in the catalog (GES and APOGEE) contained too few stars in the main sequence turnoff region to be used here. While GALAH offers only a small sample of stars overlapping with our halo sample (282 stars after quality cut), it include main sequence stars covering both blue and red sequences (133 and 125 stars, respectively), and it provides a larger overlap with the thick disc sample (1460 stars), made essentially of giant stars. The collected spectroscopic samples were used in Figure 2 to build a metallicity distribution for the blue and red sequence halo, as well as the thick disc, and in Figure 4 to explore the 3D kinematics of the samples in cylindrical coordinates.

Some quality flags were used to clean the spectroscopic samples: both were required to have a quality flag=0 in the compilation catalogue⁴³, as advised by the authors. Additionally, LAMOST stars were considered only when `snrg` ≥ 30 and GALAH stars were considered only when `flag_cannon` = 0.

4 Galaxy simulation

The simulation used for Figures 3 and 4 comes from a fully cosmological, hydrodynamical simulation of a Milky Way mass analogue galaxy from the MaGICC program¹². These simulated galaxies have been shown to match a wide variety of galaxy scaling relations over a wide mass range, as well as reproducing a range of other galaxy properties such as enrichment of the Circum-Galactic Medium⁵³. The particular realisation, g15784, has total mass of 1.4×10^{12} solar masses and has been shown to be in good agreement with the Milky Way in terms of its detailed chemical and kinematic properties of the thick and thin discs⁵⁴. In the present study we show that the stars in the region around the Sun match the most important properties of the stars observed in our own Milky Way, and use this to interpret the red and blue sequences of the observed halo CMD as belonging to the main Milky Way progenitor and Gaia-Enceladus respectively, with the merger of these two proto-galaxies resulting in the in-situ and vast majority of the inner stellar halo.

In the simulation, stars form when gas has become sufficiently cool ($T < 10,000$ K) and sufficiently dense ($n_{\text{th}} > 9.3 \text{ cm}^{-3}$). When gas particles meet these criteria, stars form according to: $dM_*/dt = c_* M_{\text{gas}}/t_{\text{dyn}}$, where M_* is the mass of stars formed in time dt , M_{gas} is the mass of a gas particle, t_{dyn} is the dynamical time of gas particles, and c_* is the star formation efficiency – i.e., the fraction of gas that will be converted into stars. Supernova feedback follows the blastwave model⁵⁵ with thermal energy (10^{51} erg) deposited to the surrounding ISM from each supernova. The simulations also include radiation feedback from massive stars⁵⁶. Cooling is disabled in the blast region (~ 100 pc) for ~ 10 Myr. The simulation includes heating from a uniform UV ionising background radiation field⁵⁷. Cooling takes into account both primordial gas and metals⁵⁸. The metal cooling grid is derived using CLOUDY⁵⁹.

Along with the fact that the same physical prescriptions used in this simulation resulted in matching scaling relations at a range of masses, meaning that low mass accreted satellites contain the correct amount of stars and gas for their halo mass, the correspondence with the observations of the thick disc gives us confidence in using this Milky Way analogue as an interpretive tool, as we do in this paper.

References

1. Searle, L. & Zinn, R. Compositions of halo clusters and the formation of the galactic halo. *Astrophys. J.* **225**, 357–379 (1978). DOI 10.1086/156499.
2. Bullock, J. S. & Johnston, K. V. Tracing Galaxy Formation with Stellar Halos. I. Methods. *Astrophys. J.* **635**, 931–949 (2005). DOI 10.1086/497422. [astro-ph/0506467](#).
3. Belokurov, V., Erkal, D., Evans, N. W., Koposov, S. E. & Deason, A. J. Co-formation of the disc and the stellar halo. *Mon. Not. R. Astron. Soc.* **478**, 611–619 (2018). DOI 10.1093/mnras/sty982. [1802.03414](#).
4. Carollo, D. *et al.* The age structure of the Milky Way’s halo. *Nat. Phys.* **12**, 1170–1176 (2016). DOI 10.1038/nphys3874. [1607.08628](#).
5. McConnachie, A. W. *et al.* The Large-scale Structure of the Halo of the Andromeda Galaxy. II. Hierarchical Structure in the Pan-Andromeda Archaeological Survey. *Astrophys. J.* **868**, 55 (2018). DOI 10.3847/1538-4357/aae8e7. [1810.08234](#).
6. Brook, C. B., Kawata, D. & Gibson, B. K. Simulating a white dwarf dominated Galactic halo. *Mon. Not. R. Astron. Soc.* **343**, 913–923 (2003). DOI 10.1046/j.1365-8711.2003.06734.x. [astro-ph/0305014](#).
7. Schuster, W. J., Moreno, E., Nissen, P. E. & Pichardo, B. Two distinct halo populations in the solar neighborhood. III. Evidence from stellar ages and orbital parameters. *Astron. Astrophys.* **538**, A21 (2012). DOI 10.1051/0004-6361/201118035. [1111.4026](#).
8. Helmi, A. *et al.* The merger that led to the formation of the Milky Way’s inner stellar halo and thick disk. *Nat.* **563**, 85–88 (2018). DOI 10.1038/s41586-018-0625-x. [1806.06038](#).
9. Gaia Collaboration *et al.* Gaia Data Release 2. Observational Hertzsprung–Russell diagrams. *Astron. Astrophys.* **616**, A10 (2018). DOI 10.1051/0004-6361/201832843. [1804.09378](#).
10. Gallart, C., Zoccali, M. & Aparicio, A. The Adequacy of Stellar Evolution Models for the Interpretation of the Color-Magnitude Diagrams of Resolved Stellar Populations. *Annu. Rev. Astron. Astrophys.* **43**, 387–434 (2005). DOI 10.1146/annurev.astro.43.072103.150608.
11. Bernard, E. J. *et al.* Star formation history of the Galactic bulge from deep HST imaging of low reddening windows. *Mon. Not. R. Astron. Soc.* **477**, 3507–3519 (2018). DOI 10.1093/mnras/sty902. [1801.01426](#).
12. Brook, C. B., Stinson, G., Gibson, B. K., Wadsley, J. & Quinn, T. MaGICC discs: matching observed galaxy relationships over a wide stellar mass range. *Mon. Not. R. Astron. Soc.* **424**, 1275–1283 (2012). DOI 10.1111/j.1365-2966.2012.21306.x. [1201.3359](#).
13. Haywood, M. *et al.* In Disguise or Out of Reach: First Clues about In Situ and Accreted Stars in the Stellar Halo of the Milky Way from Gaia DR2. *Astrophys. J.* **863**, 113 (2018). DOI 10.3847/1538-4357/aad235. [1805.02617](#).
14. Soderblom, D. R. The Ages of Stars. *Annu. Rev. Astron. Astrophys.* **48**, 581–629 (2010). DOI 10.1146/annurev-astro-081309-130806. [1003.6074](#).
15. Gallart, C., Freedman, W. L., Aparicio, A., Bertelli, G. & Chiosi, C. The Star Formation History of the Local Group Dwarf Galaxy Leo I. *Astron. J.* **118**, 2245–2261 (1999). DOI 10.1086/301078. [astro-ph/9906121](#).

16. Dolphin, A. E. Numerical methods of star formation history measurement and applications to seven dwarf spheroidals. *Mon. Not. R. Astron. Soc.* **332**, 91–108 (2002). DOI 10.1046/j.1365-8711.2002.05271.x. [astro-ph/0112331](#).
17. Aparicio, A. & Hidalgo, S. L. IAC-pop: Finding the Star Formation History of Resolved Galaxies. *Astron. J.* **138**, 558–567 (2009). DOI 10.1088/0004-6256/138/2/558. [0906.0712](#).
18. Monelli, M. *et al.* The ACS LCID Project. III. The Star Formation History of the Cetus dSph Galaxy: A Post-reionization Fossil. *Astrophys. J.* **720**, 1225–1245 (2010). DOI 10.1088/0004-637X/720/2/1225. [1002.4300](#).
19. Cignoni, M. & Tosi, M. Star Formation Histories of Dwarf Galaxies from the Colour-Magnitude Diagrams of Their Resolved Stellar Populations. *Adv. Astron.* **2010**, 158568 (2010). DOI 10.1155/2010/158568. [0909.4234](#).
20. Benedict, G. F. *et al.* Hubble Space Telescope Fine Guidance Sensor Parallaxes of Galactic Cepheid Variable Stars: Period-Luminosity Relations. *Astron. J.* **133**, 1810–1827 (2007). DOI 10.1086/511980. [astro-ph/0612465](#).
21. Beaton, R. L. *et al.* The Carnegie-Chicago Hubble Program. I. An Independent Approach to the Extragalactic Distance Scale Using Only Population II Distance Indicators. *Astrophys. J.* **832**, 210 (2016). DOI 10.3847/0004-637X/832/2/210. [1604.01788](#).
22. Hernandez, X., Valls-Gabaud, D. & Gilmore, G. The recent star formation history of the Hipparcos solar neighbourhood. *Mon. Not. R. Astron. Soc.* **316**, 605–612 (2000). DOI 10.1046/j.1365-8711.2000.03537.x. [astro-ph/0003113](#).
23. Bertelli, G. & Nasi, E. Star Formation History in the Solar Vicinity. *Astron. J.* **121**, 1013–1023 (2001). DOI 10.1086/318781.
24. Cignoni, M., Degl’Innocenti, S., Prada Moroni, P. G. & Shore, S. N. Recovering the star formation rate in the solar neighborhood. *Astron. Astrophys.* **459**, 783–796 (2006). DOI 10.1051/0004-6361:20065645. [astro-ph/0608654](#).
25. Bernard, E. J. Reconstructing the star formation history of the Solar neighbourhood with Gaia. In Chiappini, C., Minchev, I., Starkenburg, E. & Valentini, M. (eds.) *Rediscovering Our Galaxy*, vol. 334 of *IAU Symposium*, 158–161 (2018). DOI 10.1017/S1743921317008341.
26. Gaia Collaboration *et al.* Gaia Data Release 2. Summary of the contents and survey properties. *Astron. Astrophys.* **616**, A1 (2018). DOI 10.1051/0004-6361/201833051. [1804.09365](#).
27. Pietrinferni, A., Cassisi, S., Salaris, M. & Castelli, F. A Large Stellar Evolution Database for Population Synthesis Studies. II. Stellar Models and Isochrones for an α -enhanced Metal Distribution. *Astrophys. J.* **642**, 797–812 (2006). DOI 10.1086/501344. [astro-ph/0603721](#).
28. Hawkins, K., Jofré, P., Gilmore, G. & Masseron, T. On the relative ages of the α -rich and α -poor stellar populations in the Galactic halo. *Mon. Not. R. Astron. Soc.* **445**, 2575–2588 (2014). DOI 10.1093/mnras/stu1910. [1409.3431](#).
29. Erb, D. K. *et al.* The Mass-Metallicity Relation at $z \gtrsim 2$. *Astrophys. J.* **644**, 813–828 (2006). DOI 10.1086/503623. [astro-ph/0602473](#).
30. Ma, X. *et al.* The origin and evolution of the galaxy mass-metallicity relation. *Mon. Not. R. Astron. Soc.* **456**, 2140–2156 (2016). DOI 10.1093/mnras/stv2659. [1504.02097](#).

31. Behroozi, P. S., Wechsler, R. H. & Conroy, C. The Average Star Formation Histories of Galaxies in Dark Matter Halos from $z = 0-8$. *Astrophys. J.* **770**, 57 (2013). DOI 10.1088/0004-637X/770/1/57. [1207.6105](#).
32. Zolotov, A. *et al.* The Dual Origin of Stellar Halos. *Astrophys. J.* **702**, 1058–1067 (2009). DOI 10.1088/0004-637X/702/2/1058. [0904.3333](#).
33. Bonaca, A., Conroy, C., Wetzel, A., Hopkins, P. F. & Kereš, D. Gaia Reveals a Metal-rich, in situ Component of the Local Stellar Halo. *Astrophys. J.* **845**, 101 (2017). DOI 10.3847/1538-4357/aa7d0c. [1704.05463](#).
34. Fernández-Alvar, E. *et al.* Disentangling the Galactic Halo with APOGEE. II. Chemical and Star Formation Histories for the Two Distinct Populations. *Astrophys. J.* **852**, 50 (2018). DOI 10.3847/1538-4357/aa9ced. [1711.06225](#).
35. Hawkins, K., Jofré, P., Masseron, T. & Gilmore, G. Using chemical tagging to redefine the interface of the Galactic disc and halo. *Mon. Not. R. Astron. Soc.* **453**, 758–774 (2015). DOI 10.1093/mnras/stv1586. [1507.03604](#).
36. Mackereth, J. T. *et al.* The origin of accreted stellar halo populations in the Milky Way using APOGEE, Gaia, and the EAGLE simulations. *Mon. Not. R. Astron. Soc.* **482**, 3426–3442 (2019). DOI 10.1093/mnras/sty2955. [1808.00968](#).
37. Brook, C. B., Kawata, D., Gibson, B. K. & Freeman, K. C. The Emergence of the Thick Disk in a Cold Dark Matter Universe. *Astrophys. J.* **612**, 894–899 (2004). DOI 10.1086/422709. [astro-ph/0405306](#).
38. Fuhrmann, K. Nearby stars of the Galactic disc and halo - V. *Mon. Not. R. Astron. Soc.* **414**, 2893–2922 (2011). DOI 10.1111/j.1365-2966.2011.18476.x.
39. Recio-Blanco, A. *et al.* The Gaia-ESO Survey: the Galactic thick to thin disc transition. *Astron. Astrophys.* **567**, A5 (2014). DOI 10.1051/0004-6361/201322944. [1403.7568](#).
40. Haywood, M. *et al.* When the Milky Way turned off the lights: APOGEE provides evidence of star formation quenching in our Galaxy. *Astron. Astrophys.* **589**, A66 (2016). DOI 10.1051/0004-6361/201527567. [1601.03042](#).
41. Zhao, G., Zhao, Y.-H., Chu, Y.-Q., Jing, Y.-P. & Deng, L.-C. LAMOST spectral survey – An overview. *Res. Astron. Astrophys.* **12**, 723–734 (2012). DOI 10.1088/1674-4527/12/7/002.
42. Buder, S. *et al.* The GALAH Survey: second data release. *Mon. Not. R. Astron. Soc.* **478**, 4513–4552 (2018). DOI 10.1093/mnras/sty1281. [1804.06041](#).
43. Sanders, J. L. & Das, P. Isochrone ages for 3 million stars with the second Gaia data release. *Mon. Not. R. Astron. Soc.* **481**, 4093–4110 (2018). DOI 10.1093/mnras/sty2490. [1806.02324](#).
44. Luri, X. *et al.* Gaia Data Release 2. Using Gaia parallaxes. *Astron. Astrophys.* **616**, A9 (2018). DOI 10.1051/0004-6361/201832964. [1804.09376](#).
45. Lallement, R. *et al.* Three-dimensional maps of interstellar dust in the Local Arm: using Gaia, 2MASS, and APOGEE-DR14. *Astron. Astrophys.* **616**, A132 (2018). DOI 10.1051/0004-6361/201832832. [1804.06060](#).
46. Casagrande, L. & Vandenberg, D. A. On the use of Gaia magnitudes and new tables of bolometric corrections. *Mon. Not. R. Astron. Soc.* **479**, L102–L107 (2018). DOI 10.1093/mnrasl/sly104. [1806.01953](#).

47. Ruiz-Lara, T. *et al.* Integrated-light analyses vs. colour-magnitude diagrams. II. Leo A: an extremely young dwarf in the Local Group. *Astron. Astrophys.* **617**, A18 (2018). DOI 10.1051/0004-6361/201732398. [1805.04323](#).
48. Bernard, E. J. *et al.* The spatially-resolved star formation history of the M31 outer disc. *Mon. Not. R. Astron. Soc.* **453**, L113–L117 (2015). DOI 10.1093/mnras/slv116. [1508.01559](#).
49. Pietrinferni, A., Cassisi, S., Salaris, M. & Castelli, F. A Large Stellar Evolution Database for Population Synthesis Studies. I. Scaled Solar Models and Isochrones. *Astrophys. J.* **612**, 168–190 (2004). DOI 10.1086/422498. [astro-ph/0405193](#).
50. Kroupa, P., Tout, C. A. & Gilmore, G. The distribution of low-mass stars in the Galactic disc. *Mon. Not. R. Astron. Soc.* **262**, 545–587 (1993). DOI 10.1093/mnras/262.3.545.
51. Evans, D. W. *et al.* Gaia Data Release 2. Photometric content and validation. *Astron. Astrophys.* **616**, A4 (2018). DOI 10.1051/0004-6361/201832756. [1804.09368](#).
52. Hidalgo, S. L. *et al.* The ACS LCID Project. V. The Star Formation History of the Dwarf Galaxy LGS-3: Clues to Cosmic Reionization and Feedback. *Astrophys. J.* **730**, 14 (2011). DOI 10.1088/0004-637X/730/1/14. [1101.5762](#).
53. Stinson, G. S. *et al.* MAGICC haloes: confronting simulations with observations of the circumgalactic medium at $z=0$. *Mon. Not. R. Astron. Soc.* **425**, 1270–1277 (2012). DOI 10.1111/j.1365-2966.2012.21522.x. [1112.1698](#).
54. Miranda, M. S. *et al.* Origin of the metallicity distribution in the thick disc. *Astron. Astrophys.* **587**, A10 (2016). DOI 10.1051/0004-6361/201525789. [1512.04559](#).
55. Stinson, G. *et al.* Star formation and feedback in smoothed particle hydrodynamic simulations - I. Isolated galaxies. *Mon. Not. R. Astron. Soc.* **373**, 1074–1090 (2006). DOI 10.1111/j.1365-2966.2006.11097.x. [astro-ph/0602350](#).
56. Stinson, G. S. *et al.* Making Galaxies In a Cosmological Context: the need for early stellar feedback. *Mon. Not. R. Astron. Soc.* **428**, 129–140 (2013). DOI 10.1093/mnras/sts028. [1208.0002](#).
57. Haardt, F. & Madau, P. Radiative Transfer in a Clumpy Universe. II. The Ultraviolet Extragalactic Background. *Astrophys. J.* **461**, 20 (1996). DOI 10.1086/177035. [astro-ph/9509093](#).
58. Shen, S., Wadsley, J. & Stinson, G. The enrichment of the intergalactic medium with adiabatic feedback - I. Metal cooling and metal diffusion. *Mon. Not. R. Astron. Soc.* **407**, 1581–1596 (2010). DOI 10.1111/j.1365-2966.2010.17047.x. [0910.5956](#).
59. Ferland, G. J. *et al.* CLOUDY 90: Numerical Simulation of Plasmas and Their Spectra. *Publ. Astron. Soc. Pac.* **110**, 761–778 (1998). DOI 10.1086/316190.

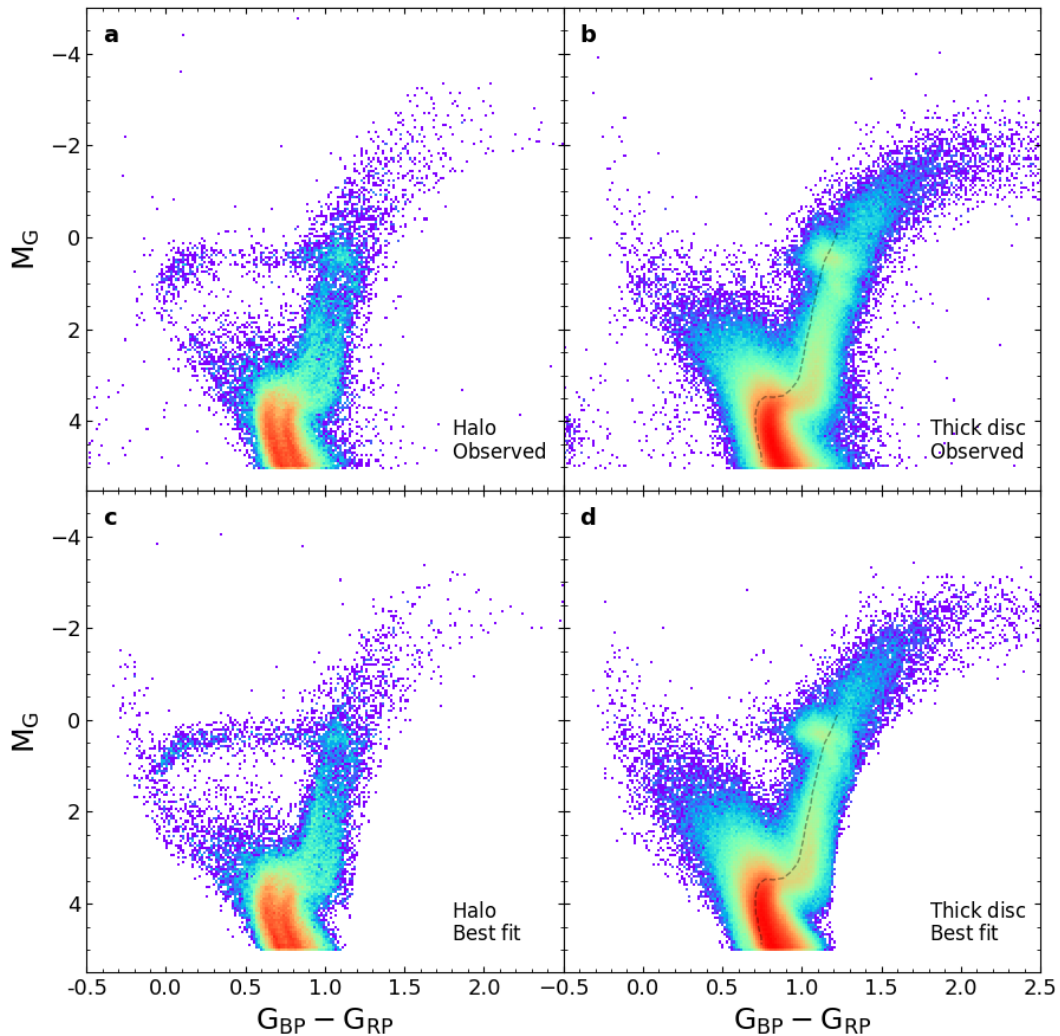


Figure 1. Milky Way halo and thick disc Colour-Magnitude Diagrams (CMDs). Panels **a** and **b** display the observed Gaia CMDs for the halo and thick disc sub-populations, respectively. They have been represented as Hess diagrams with a logarithmic normalization of the number of stars in the colour-magnitude bins. Two sequences are clear in panel **a**: the blue sequence on the left and the red sequence on the right. Panels **c** and **d** display the best-fit models to the halo and thick disc CMDs, respectively. The dashed line in panels **b** and **d** indicates the position of the gap between the blue and red halo sequences. See Methods for more information on the sample selection and the CMD fitting technique.

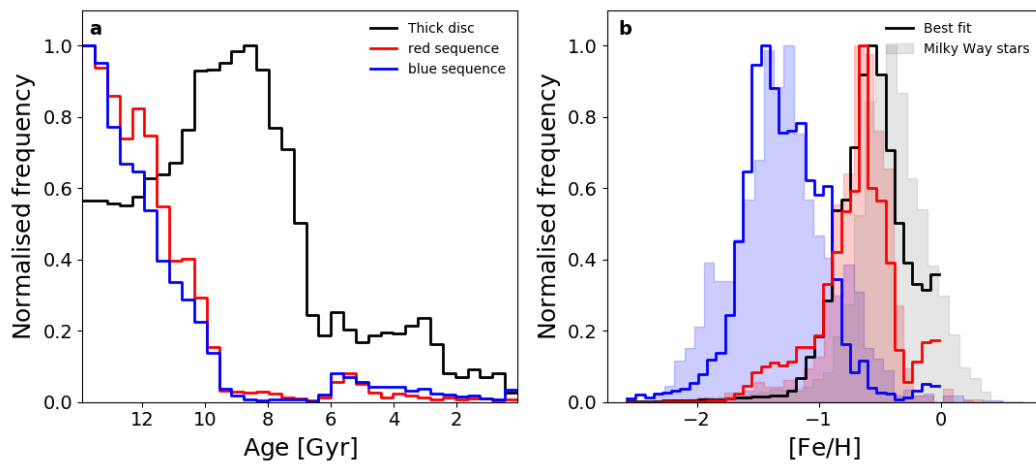


Figure 2. Milky Way halo and thick disc stellar age and iron [Fe/H] distributions. Panel **a** shows the distribution of stellar ages of the thick disc (grey histogram), blue (blue histogram) and red (red histogram) halo sequences according to their best-fit model CMDs. Panel **b** shows the distribution of [Fe/H], of the best-fitting models for the blue and red halo sequences as well as the thick disc stars (solid lines) compared to those derived using LAMOST and GALAH spectroscopy^{41–43}, for the same populations (filled histograms). The good agreement between the [Fe/H] distributions inferred with the CMD fitting technique and those measured spectroscopically provides an external check of the reliability of the results.

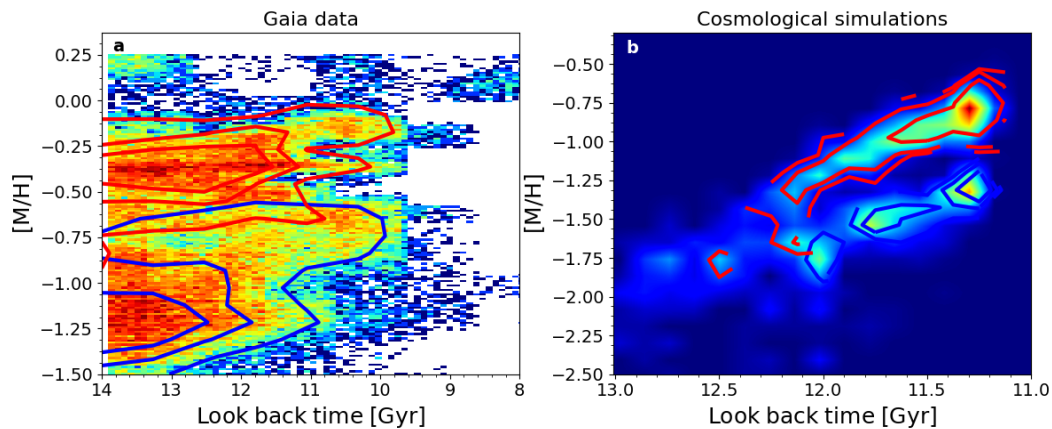


Figure 3. Age-metallicity relations for the two halo populations as compared to a simulated Milky Way analogue. Panel **a**: age-metallicity relation for the best-fit model of the halo CMD. The blue and red contours outline the distribution of stars in the blue and red halo sequences, respectively, overlaid to the general distribution of halo stars. Panel **b**, same as **a** but for a simulated Milky Way analogue (see Methods). Blue and red contours depict the age-metallicity distribution of simulated stellar particles belonging to an accreted galaxy (analogue to Gaia-Enceladus) and the Galaxy progenitor, respectively. The last major merger can be identified as two tracks in the age-metallicity plot, with the higher metallicity stars belonging to the main progenitor and the lower metallicity stars coming from the merged satellite. The agreement, only expected to be qualitative, is remarkable. The time and mass of the last major merger, which can be seen to differ between the simulation and the real Milky Way, determine the details of the ages and metallicities of the red and blue halo populations.

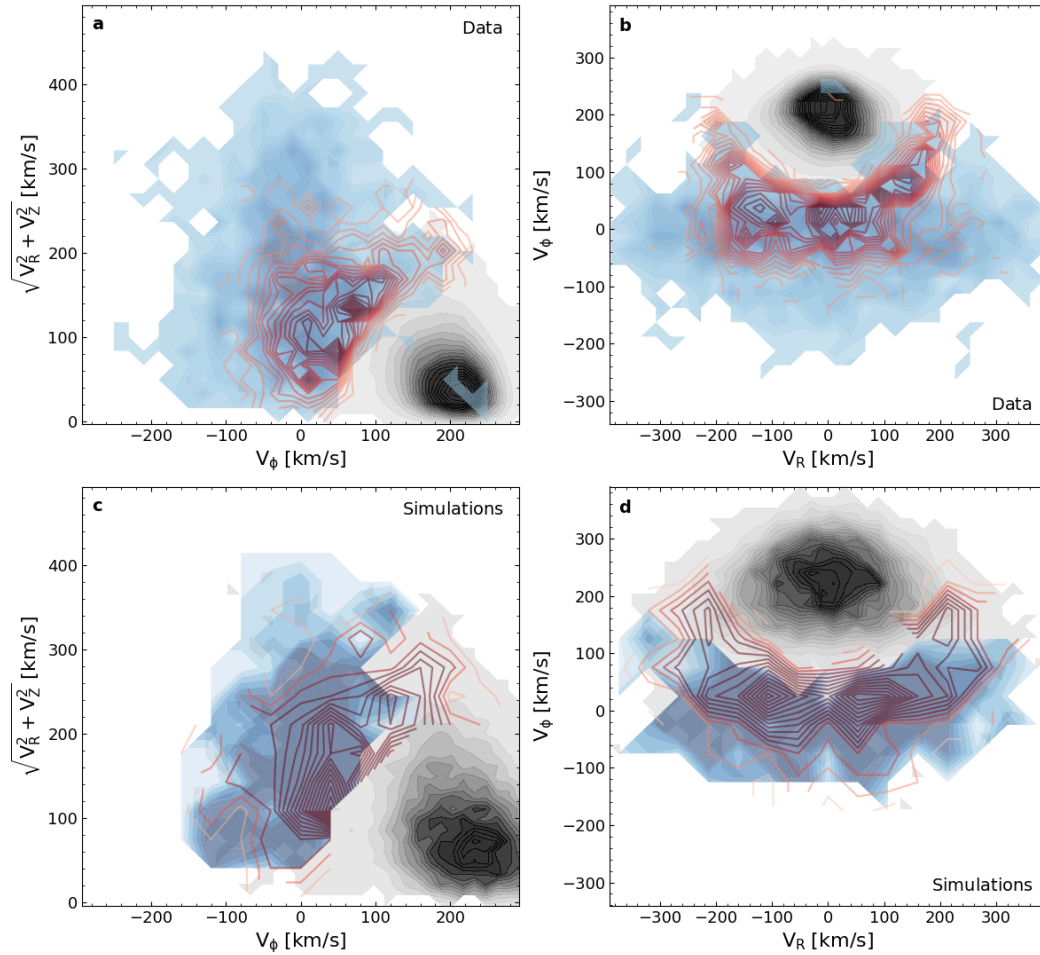


Figure 4. Comparison of the stellar kinematics between observations of Milky Way stars and the simulated Milky Way analogue. **a** and **c** show the Toomre Diagram for Milky Way stars (obtained by combining Gaia DR2 astrometry and LAMOST radial velocities⁴³), and for the simulated Milky Way analogue galaxy, respectively. **b** and **d** display similar information but in an azimuthal velocity (V_ϕ) versus radial velocity (V_R) diagram. In the four panels, stars belonging to the observed halo blue sequence or the simulated accreted satellite are represented by blue shades, the observed halo red sequence or the simulated progenitor as red contours, and observed or simulated thick disc in grey scale. Note that some stars in our halo sample turn out to have disc properties when the full kinematic information is taken into account. This can help explain the presence of a small fraction of young stars in the halo sequences (panel a of Figure 2) as contamination from thin disc stars in the sample. The same is true for the inferred thick disc young population.